

Coherent photon–photon processes in disruptive and non-disruptive relativistic heavy-ion collisions

G. Baur, N. Baron

Institut für Kernphysik (Theorie), Forschungszentrum Jülich, D 5170 Jülich, Germany

Received 2 June 1992

(Revised 1 February 1993)

Abstract

Using an impact parameter formulation, differential probability distributions and cross sections for the production of lepton pairs via the photon–photon mechanism are calculated for relativistic heavy-ion collisions. The characteristic features of lepton pair production in disruptive as well as in non-disruptive A – A collisions are studied. Cross sections can be large, the very low k_{\perp} -values of the pairs will help to distinguish these pairs from the ones originating from other sources like Drell–Yan or thermal production.

1. Introduction

Dileptons play a very important role in the diagnostics of the hot hadronic matter formed in relativistic heavy-ion collisions. There are various physical sources which contribute, like the Drell–Yan mechanism, preequilibrium pairs or thermal emission of lepton pairs from the quark–gluon-plasma. Many theoretical models have been and will be studied, see e.g. refs. [1,2].

Soon after the discovery of the positron, the production of e^+e^- pairs in relativistic heavy-ion collisions via the $\gamma\gamma$ mechanism was studied theoretically [3]. Due to coherence, total cross sections for e^+e^- production are large. This process has been studied more closely in recent years (see e.g. refs. [4–7]). The study of the more differential aspects of lepton pair production in relativistic heavy-ion collisions via the $\gamma\gamma$ mechanism is of continuing relevance.

It is of special interest to investigate the dependence of the $\gamma\gamma$ mechanism on the impact parameter b of the colliding nuclei:

(i) In central, disruptive collisions with impact parameter $b < R_1 + R_2$ (the sum of the nuclear radii), coherent pairs are a potential background to the other mechanisms.

Correspondence to: Prof. Dr. G. Baur, Institut für Kernphysik (Theorie), Forschungszentrum Jülich, W-5170 Jülich, Germany.

(ii) In non-disruptive collisions (i.e. $b > R_1 + R_2$), the $\gamma\gamma$ process can be studied in its pure form.

In sect. 2 the impact parameter formulation of the $\gamma\gamma$ process is given in detail. A brief outline of this method was given in ref. [8]. In order to expose clearly the b -dependence of the process and also to simplify numerical calculations it is found advantageous to work with impact-parameter-dependent equivalent photon spectra. This is in contrast to the usual theoretical framework for $\gamma\gamma$ processes in e^+e^- collisions (see e.g. ref. [9]). In the usual quantum-mechanical plane-wave approach the impact parameter of the system does not appear explicitly. This is a problem for the distinction between disruptive and non-disruptive collisions which occur in the heavy-ion case. The impact-parameter method was first formulated in ref. [10] and numerical calculations were done in refs. [11–14] along these lines.

The impact parameter dependence of Higgs-production via the $\gamma\gamma$ mechanism is also studied in ref. [15]. A recent summary of electromagnetic pair production is given in ref. [16].

In sect. 3 our numerical results are given and discussed. In principle any $\gamma\gamma$ -induced process including angular distributions can be studied. We concentrate here on lepton pair production at SPS, RHIC and LHC energies. Differential probability distributions and cross sections are calculated to show the main features of the process. We suggest a procedure for off-shell corrections in the equivalent photon approximation and study a smooth cut-off model for strong absorption effects. Our conclusions are given in sect. 4.

2. Theory: impact parameter dependence of the $\gamma\gamma$ process

A recipe for the calculation of $\gamma\gamma$ processes in the impact parameter formulation was given in ref. [10]. The probability for a $\gamma\gamma \rightarrow f$ process in a collision with impact parameter b can be obtained by folding the impact-parameter-dependent equivalent photon spectra $N(\omega, b)$ in the following way:

$$\frac{d^2P}{d\omega_1 d\omega_2} = \iint d^2\mathbf{b}_1 d^2\mathbf{b}_2 \delta^2(\mathbf{b} + \mathbf{b}_2 - \mathbf{b}_1) N(\omega_1, b_1) N(\omega_2, b_2) \frac{1}{\omega_1 \omega_2} \\ \times (\cos^2\varphi \sigma_{\parallel} + \sin^2\varphi \sigma_{\perp}). \quad (2.1)$$

The equivalent photon spectra in the ultra-relativistic limit are given by [17]:

$$N(\omega, b) = \frac{Z^2 \alpha^2}{\pi^2} \frac{\Phi(x, b)}{b^2} \quad (2.2a)$$

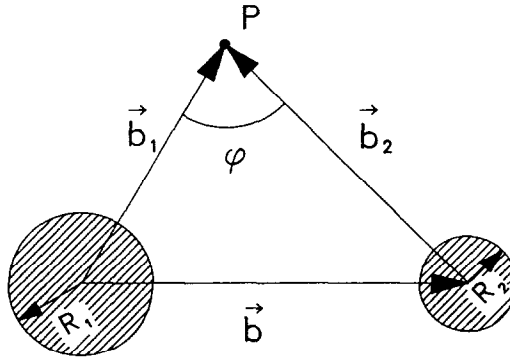


Fig. 1. View perpendicular to the direction of motion of the two ions. In a semiclassical picture the two equivalent photons of energy ω_1 and ω_2 collide in a point P with distance b_1 from ion 1 and b_2 from ion 2. The impact parameter b is the distance between the colliding nuclei with radius R_1 and R_2 .

with

$$\Phi(x, b) = \left| \int_0^\infty du u^2 J_1(u) \frac{f[-(x^2 + u^2)/b^2]}{x^2 + u^2} \right|^2, \quad (2.2b)$$

where x is the dimensionless scaling variable defined by $x = \omega b / \gamma v$ and f denotes the electromagnetic form factor of the (spinless) nucleus. The angle between b_1 and b_2 is denoted by φ (see fig. 1), σ_{\parallel} and σ_{\perp} are the cross sections for parallel and perpendicular polarizations of the photons.

The final state is characterized by its total four momentum $k = (\varepsilon, \mathbf{k}_{\perp}, k_3)$. It is related to the energy ω_1 and ω_2 of the equivalent photons by $k_3 = \omega_1 - \omega_2$, $\varepsilon = \omega_1 + \omega_2$. The invariant mass M and the rapidity Y of the final systems are given by $M \cong 4\omega_1\omega_2$ and $Y \cong \frac{1}{2} \ln(\omega_1/\omega_2)$.

It will now be shown how this formula is obtained within the semiclassical method. Actually the derivation of this formula appears to be quite involved, therefore we give the essential steps in the following. Up to now, transverse momenta were not considered. The present approach also allows a computation of transverse momentum distributions, as will be shown below.

We consider the classical straight-line motion of two relativistic heavy ions with impact parameter b (see fig. 2). The electromagnetic fields accompanying the ions with charges Z_1 and Z_2 will give rise to $\gamma\gamma$ processes leading to a final state f with particles j of momentum p_j . The sum of these momenta is given by $k = \sum_{j \in f} p_j$, the total four momentum of the final state. To a very good approximation the electromagnetic potentials of the ultra-relativistic heavy ions can be

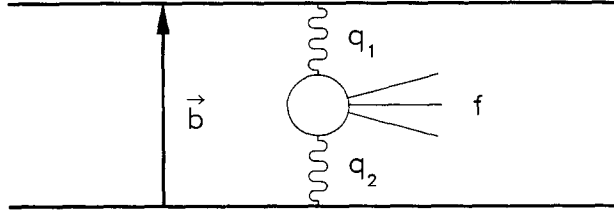


Fig. 2. Two relativistic heavy ions move on straight-line trajectories with impact parameter b . The equivalent photons with four-momentum q_1 and q_2 produce a final state f with total four-momentum $k = q_1 + q_2$.

considered as external classical fields. They are given by (see e.g. ref. [18]):

$$\begin{aligned}
 a_\mu(q) &= A_{1\mu}(q) + A_{2\mu}(q) \\
 &= 8\pi^2 eZ_1 \frac{f_1(q^2)}{q^2} \delta(qU^{(1)}) U_\mu^{(1)} \\
 &\quad + 8\pi^2 eZ_2 \frac{f_2(q^2)}{q^2} \delta(qU^{(2)}) e^{-iq \cdot b} U_\mu^{(2)},
 \end{aligned} \tag{2.3}$$

where $U_\mu^{(i)}$, $i = 1, 2$ are the four-velocities of the heavy ions. We use a coordinate system where the ions move with opposite velocities in the z -direction, i.e. $U_\mu^{(1)} = (\gamma, 0, 0, \gamma v)$ and $U_\mu^{(2)} = (\gamma, 0, 0, -\gamma v)$.

Quite generally the amplitude for the process $\gamma\gamma \rightarrow f$ can be written as [19]

$$\langle f | T | \gamma_1 \gamma_2 \rangle = \epsilon_1^{\mu_1} \epsilon_2^{\mu_2} M^{\mu_1 \mu_2}, \tag{2.4}$$

where ϵ_1 and ϵ_2 denote the polarization vectors of the virtual photons. The total dynamical information of the process is contained in the tensor $M^{\mu_1 \mu_2}$. For the calculation of cross sections it is convenient to define a tensor $W^{\mu_1 \mu_2 \nu_1 \nu_2}$ (see refs. [9,19]) by

$$W^{\mu_1 \nu_1 \mu_2 \nu_2} = \sum_{\text{pol} \in f} \int \prod_{j \in f} \frac{d^3 \mathbf{p}_j}{(2\pi)^3} \frac{N_j}{E_j} (2\pi)^4 \delta^{(4)}(q_1 + q_2 - k) M^{\mu_1 \nu_1} M^{*\mu_2 \nu_2}, \tag{2.5}$$

where q_1 and q_2 are the four-momenta of the photons. The factor N_j/E_j is the normalization factor of particle j , i.e. $N_j = \frac{1}{2}$ for bosons and $N_j = M_j$ for non-zero mass fermions. The summation over the polarizations and the integration over the phase-space of all particles belonging to f in eq. (2.5) is related to the $\gamma\gamma$ total cross section in a well-known way [9,19].

The matrix element of the process

$$Z_1 + Z_2 \rightarrow Z_1 + Z_2 + f(k) \quad (2.6)$$

producing a state f with total four-momentum k via the $\gamma\gamma$ mechanism is given by

$$S_{i \rightarrow f} = \iint \frac{d^4 q_1}{(2\pi)^4} \frac{d^4 q_2}{(2\pi)^4} (2\pi)^4 \delta^{(4)}(q_1 + q_2 - k) A_{1\mu_1}(q_1) A_{2\mu_2}(q_2) M^{\mu_1\mu_2}. \quad (2.7)$$

The four-potentials $A_{i\mu_i}$ are proportional to the four-velocities $U_{\mu_i}^{(i)}$ [see eq. (2.3)]. By using gauge invariance we can transform these vectors into vectors which are transversal, i.e. perpendicular to the z -direction. The gauge-invariance condition in momentum-space reads

$$A_\mu(q) \rightarrow \tilde{A}_\mu(q) = A_\mu(q) + \Lambda q_\mu, \quad (2.8)$$

where Λ is a scalar function. The requirement of transversality leads in the ultra-relativistic limit to four-potentials (suppressing the tilde)

$$A_{i\mu}(q) = -8\pi^2 e Z_i \frac{f_i(q_i^2)}{q_i^2} \frac{\gamma}{\omega_i} \delta(q U^{(i)}) q_{i\mu}; \quad \mu = 1, 2. \quad (2.9)$$

With these transformed potentials we can write in the ultra-relativistic limit

$$S_{i \rightarrow f} = \frac{\gamma^2}{\omega_1 \omega_2} \iint d^4 q_1 d^4 q_2 4Z_1 Z_2 e^2 \frac{f_1(q_1^2) f_2(q_2^2)}{q_1^2 q_2^2} \times \delta(q_1 U^{(1)}) \delta(q_2 U^{(2)}) e^{-iq_2 \cdot b} q_{1\mu_1} q_{2\mu_2} M^{\mu_1\mu_2}, \quad (2.10)$$

where the indices μ_i take the values 1, 2.

The probability $dP(b)$ to form a final state with total four-momentum between k and $k + dk$ is given by:

$$dP(b) = d^4 k \sum_{\text{pol} \in f} \int \prod_{j \in f} \frac{d^3 p_j}{(2\pi)^3} \frac{N_j}{E_j} (2\pi)^4 \delta^{(4)}\left(\sum_{j \in f} p_j - k\right) |S_{i \rightarrow f}|^2. \quad (2.11)$$

This can be expressed in terms of the tensor $W^{\mu_1\mu_2\nu_1\nu_2}$ [see eq. (2.5)] as

$$dP(b) = d^4 k \iiint d^4 q_1 d^4 q_2 d^4 q'_1 d^4 q'_2 \delta^{(4)}(q_1 + q_2 - k) \times \delta^{(4)}(q'_1 + q'_2 - k) A_{1\mu_1}(q_1) A_{2\mu_2}(q_2) A_{1\nu_1}^*(q'_1) A_{2\nu_2}^*(q'_2) W^{\mu_1\mu_2\nu_1\nu_2} \quad (2.12)$$

The integrals over dq_{i0} and dq_{i3} can be carried out directly and we are left with integrals over transverse components only (we suppress the index \perp for q_i in the following):

$$\begin{aligned}
 dP(b) &= d\varepsilon d^2\mathbf{k}_\perp dk_3 \frac{(8\pi^2)^4 (Z_1 Z_2 e^2)^2}{\omega_1^2 \omega_2^2} \\
 &\times \iiint d^2q_1 d^2q_2 d^2q'_1 d^2q'_2 \delta^{(2)}(\mathbf{q}_1 + \mathbf{q}_2 - \mathbf{k}_\perp) \delta^{(2)}(\mathbf{q}'_1 + \mathbf{q}'_2 - \mathbf{k}_\perp) \\
 &\times f_1 \left[\left(\frac{\omega_1}{\gamma} \right)^2 + q_1^2 \right] f_2 \left[\left(\frac{\omega_2}{\gamma} \right)^2 + q_2^2 \right] f_1 \left[\left(\frac{\omega_1}{\gamma} \right)^2 + q_1'^2 \right] f_2 \left[\left(\frac{\omega_2}{\gamma} \right)^2 + q_2'^2 \right] \\
 &\times e^{ib \cdot (\mathbf{q}'_2 - \mathbf{q}_2)} \frac{q_{1\mu_1} q_{2\mu_2} q'_{1\nu_1} q'_{2\nu_2} W^{\mu_1 \mu_2 \nu_1 \nu_2}}{\left[\left(\frac{\omega_1}{\gamma} \right)^2 + q_1^2 \right] \left[\left(\frac{\omega_2}{\gamma} \right)^2 + q_2^2 \right] \left[\left(\frac{\omega_1}{\gamma} \right)^2 + q_1'^2 \right] \left[\left(\frac{\omega_2}{\gamma} \right)^2 + q_2'^2 \right]}
 \end{aligned} \tag{2.13}$$

In principle the tensor $W^{\mu_1 \mu_2 \nu_1 \nu_2}$ depends also on the transverse kinematical variables; in the equivalent-photon approximation we neglect this dependence. The tensor $W^{\mu_1 \mu_2 \nu_1 \nu_2}$ can be expressed in terms of $\gamma\gamma$ cross sections [9,19]. Restricting ourselves only to transverse photons we obtain in the c.m. system of the photons (see eq. 5.7 of ref. [9]):

$$\begin{aligned}
 q_{1\mu_1} q_{2\mu_2} q'_{1\nu_1} q'_{2\nu_2} W^{\mu_1 \mu_2 \nu_1 \nu_2} &= M^2 \left\{ \sigma_{\parallel} q_{1x} q_{2x} q'_{1x} q'_{2x} + \sigma_{\perp} q_{1x} q_{2y} q'_{1x} q'_{2y} \right. \\
 &\quad \left. + \left[\frac{1}{2}(\sigma_{\parallel} - \sigma_{\perp}) + \tau_a \right] q_{1x} q_{2x} q'_{1y} q'_{2y} \right. \\
 &\quad \left. + \left[\frac{1}{2}(\sigma_{\parallel} - \sigma_{\perp}) - \tau_a \right] q_{1y} q_{2x} q'_{1x} q'_{2y} + X \leftrightarrow Y \right\}.
 \end{aligned} \tag{2.14}$$

The transverse momentum distribution in c.m. coordinates of the photons can be

calculated from eq. (2.13). It may be expressed in terms of tensors T_{ij} , $i, j = x, y$:

$$\begin{aligned}
 T_{ij} &= e^{i\mathbf{b} \cdot \mathbf{k}_\perp / 2} \int d^2\mathbf{q} e^{i\mathbf{b} \cdot \mathbf{q}} \\
 &\times \frac{f_1 \left[\left(\frac{\omega_1}{\gamma} \right)^2 + \left(\frac{1}{2} \mathbf{k}_\perp + \mathbf{q} \right)^2 \right] f_2 \left[\left(\frac{\omega_2}{\gamma} \right)^2 + \left(\frac{1}{2} \mathbf{k}_\perp - \mathbf{q} \right)^2 \right] \left(\frac{1}{2} \mathbf{k} + \mathbf{q} \right)_i \left(\frac{1}{2} \mathbf{k}_\perp - \mathbf{q} \right)_j}{\left[\left(\frac{\omega_1}{\gamma} \right)^2 + \left(\frac{1}{2} \mathbf{k}_\perp + \mathbf{q} \right)^2 \right] \left[\left(-\frac{\omega_2}{\gamma} \right)^2 + \left(\frac{1}{2} \mathbf{k}_\perp - \mathbf{q} \right)^2 \right]} .
 \end{aligned} \tag{2.15}$$

We expect a transverse momentum distribution which is sharply peaked around zero. This will be discussed in detail in sect. 3.1.

Integrating over the transverse momentum \mathbf{k}_\perp we obtain

$$\begin{aligned}
 dP(\mathbf{b}) &= d\varepsilon dk_3 \frac{4(Z_1 Z_2 e^2)^2}{\omega_1 \omega_2} \\
 &\times \iiint d^2\mathbf{q}_1 d^2\mathbf{q}_2 d^2\mathbf{q}'_1 d^2\mathbf{q}'_2 \delta^{(4)}(\mathbf{q}_1 + \mathbf{q}_2 - \mathbf{q}'_1 - \mathbf{q}'_2) e^{i\mathbf{b} \cdot (\mathbf{q}'_2 - \mathbf{q}_2)} \\
 &\times f_1 \left[\left(\frac{\omega_1}{\gamma} \right)^2 + q_1^2 \right] f_2 \left[\left(\frac{\omega_2}{\gamma} \right)^2 + q_2^2 \right] f_1 \left[\left(\frac{\omega_1}{\gamma} \right)^2 + q_1'^2 \right] f_2 \left[\left(\frac{\omega_2}{\gamma} \right)^2 + q_2'^2 \right] \\
 &\times \frac{q_{1\mu_1} q_{2\mu_2} q'_{1\nu_1} q'_{2\nu_2} W^{\mu_1 \mu_2 \nu_1 \nu_2}}{\left[\left(\frac{\omega_1}{\gamma} \right)^2 + q_1^2 \right] \left[\left(\frac{\omega_2}{\gamma} \right)^2 + q_2^2 \right] \left[\left(\frac{\omega_1}{\gamma} \right)^2 + q_1'^2 \right] \left[\left(\frac{\omega_2}{\gamma} \right)^2 + q_2'^2 \right]} .
 \end{aligned} \tag{2.16}$$

In order to show the equivalence to eq. (2.1) we introduce the vectors \mathbf{b}_1 and $\mathbf{b}_2 = \mathbf{b}_1 - \mathbf{b}$ (see fig. 1). Replacing the δ -function in eq. (2.16) by an integral and changing the integration leads to:

$$\begin{aligned}
 dP(\mathbf{b}) &= d\varepsilon dk_3 \frac{(Z_1 Z_2 e^2)^2}{\pi^2} \frac{1}{\omega_1 \omega_2} \\
 &\times \iint d^2\mathbf{b}_1 d^2\mathbf{b}_2 \delta^{(2)}(\mathbf{b} + \mathbf{b}_2 - \mathbf{b}_1) \iiint d^2\mathbf{q}_1 d^2\mathbf{q}_2 d^2\mathbf{q}'_1 d^2\mathbf{q}'_2
 \end{aligned}$$

$$\begin{aligned} & \times f_1 \left[\left(\frac{\omega_1}{\gamma} \right)^2 + q_1^2 \right] f_2 \left[\left(\frac{\omega_2}{\gamma} \right)^2 + q_2^2 \right] f_1 \left[\left(\frac{\omega_1}{\gamma} \right)^2 + q_1'^2 \right] f_2 \left[\left(\frac{\omega_2}{\gamma} \right)^2 + q_2'^2 \right] \\ & \times \frac{e^{ib_1 \cdot (q_1' - q_1)} e^{ib_2 \cdot (q_2' - q_2)} q_{1\mu_1} q_{2\mu_2} q'_{1\nu_1} q'_{2\nu_2} W^{\mu_1 \mu_2 \nu_1 \nu_2}}{\left[\left(\frac{\omega_1}{\gamma} \right)^2 + q_1^2 \right] \left[\left(\frac{\omega_2}{\gamma} \right)^2 + q_2^2 \right] \left[\left(\frac{\omega_1}{\gamma} \right)^2 + q_1'^2 \right] \left[\left(\frac{\omega_2}{\gamma} \right)^2 + q_2'^2 \right]}. \end{aligned} \tag{2.17}$$

The integrals over the transverse momenta can be carried out and the result can be expressed in terms of the equivalent photon spectra eq. (2.2a, 2.2b).

In order to obtain eq. (2.1) from eq. (2.17) explicitly, eq. (2.14) is used. Taking into account that the integration over the transverse momenta in eq. (2.17) factorizes into four two-dimensional integrals and putting \mathbf{b}_1 parallel to the x -axis for convenience, we are left only with integrals of the type (the integrals containing q_{1y} and q'_{1y} vanish):

$$I_{\{y\}}^{\{x\}} = \int d^2 \mathbf{q}_2 \frac{e^{ib_2 \cdot q_2} q_{2\{y\}}}{\left(\frac{\omega}{\gamma} \right)^2 + q_2^2} f \left[\left(\frac{\omega}{\gamma} \right)^2 + q_2^2 \right]. \tag{2.18}$$

They can be evaluated using polar coordinates. We obtain

$$I_{\{y\}}^{\{x\}} = \begin{Bmatrix} \cos \phi \\ \sin \phi \end{Bmatrix} \int_0^\infty \frac{q^2 dq}{q^2 + \left(\frac{\omega}{\gamma} \right)^2} J_1(b_2 q) f \left[\left(\frac{\omega}{\gamma} \right)^2 + q^2 \right]. \tag{2.19}$$

Our results clearly establish the relation between the general eq. (2.11) and the impact-parameter-dependent equivalent-photon result eq. (2.1) and eq. (2.2a) given in ref. [10]. We want to stress at this point that the equations of sect. 2 are valid in the ultra-relativistic limit, i.e. $v \cong c$.

3. Numerical results and discussion

In the main part of sect. 3 we restrict ourselves to coherent $\gamma\gamma$ lepton pair production in ultra-relativistic heavy-ion collisions, namely the process

$$Z + Z \rightarrow Z + Z + l^+ l^-. \tag{3.1}$$

We concentrate on ^{208}Pb – ^{208}Pb collisions at SPS, RHIC and LHC energies. Of course, our assumption of straight-line motion has to be critically examined for the case of central collisions. At RHIC and LHC energies, where one can largely expect transparency, the charges, which are responsible for the electromagnetic fields, essentially pass through each other and our assumption can be considered as a reasonable starting point. At lower energies, in the energy range of SPS, stopping effects will become important. This leads to bremsstrahlung pair production and a modification of the equivalent photon spectra. These points are currently being investigated [20], but are beyond the scope of the present paper. In any case, it can be concluded from these investigations that our straight-line model is a reasonable starting point.

3.1. Transverse momentum distribution

In order to analyse the properties of the transverse momentum distribution of the created system, we rewrite eq. (2.13) in terms of a tensor $\Theta_{\mu_1\mu_2\nu_1\nu_2}$ leading to:

$$dP(b) = d\varepsilon dk_3 d^2k_\perp \frac{(8\pi^2)^2 (Z_1 Z_2 e^2)^2}{\omega_1^2 \omega_2^2} \Theta_{\mu_1\mu_2\nu_1\nu_2} W^{\mu_1\mu_2\nu_1\nu_2}. \quad (3.2)$$

The tensor $\Theta_{\mu_1\mu_2\nu_1\nu_2}$ in eq. (3.2) is given explicitly by:

$$\begin{aligned} & \Theta_{\mu_1\mu_2\nu_1\nu_2}(\omega_1, \omega_2, \mathbf{b}, \mathbf{k}_\perp) \\ &= \int d^2q_1 d^2q_2 d^2q'_1 d^2q'_2 \delta^{(2)}(\mathbf{q}_1 + \mathbf{q}_2 - \mathbf{k}_\perp) \delta^{(2)}(\mathbf{q}'_1 + \mathbf{q}'_2 - \mathbf{k}_\perp) \\ & \times f_1 \left[\left(\frac{\omega_1}{\gamma} \right)^2 + q_1^2 \right] f_2 \left[\left(\frac{\omega_2}{\gamma} \right)^2 + q_2^2 \right] f_1 \left[\left(\frac{\omega_1}{\gamma} \right)^2 + q_1'^2 \right] f_2 \left[\left(\frac{\omega_2}{\gamma} \right)^2 + q_2'^2 \right] \\ & \times e^{i\mathbf{b} \cdot (\mathbf{q}'_2 - \mathbf{q}_2)} \frac{q_{1\mu_1} q_{2\mu_2} q'_{1\nu_1} q'_{2\nu_2}}{\left[\left(\frac{\omega_1}{\gamma} \right)^2 + q_1^2 \right] \left[\left(\frac{\omega_2}{\gamma} \right)^2 + q_2^2 \right] \left[\left(\frac{\omega_1}{\gamma} \right)^2 + q_1'^2 \right] \left[\left(\frac{\omega_2}{\gamma} \right)^2 + q_2'^2 \right]}. \end{aligned} \quad (3.3)$$

Since the momentum distribution depends only on the angle between \mathbf{b} and \mathbf{k}_\perp , we can put \mathbf{b} , without loss of generality, into the direction of the x -axis. Using the symmetry of $\Theta_{\mu_1\mu_2\nu_1\nu_2}$ in the primed and unprimed variables and introducing another integration like in eq. (2.17) one can show:

$$\Theta_{\mu_1\mu_2\nu_1\nu_2} \equiv 0 \quad \text{for } \mu_1 = y \vee \nu_1 = y. \quad (3.4)$$

With the tensor decomposition of $W^{\mu_1\mu_2\nu_1\nu_2}$ of ref. [9] we obtain (keeping only transverse photons)

$$\Theta_{\mu_1\mu_2\nu_1\nu_2}W^{\mu_1\mu_2\nu_1\nu_2} = (\Theta_{xxxx} + Q_{xyxy})W_{\text{TT}} + \frac{1}{2}(\Theta_{xxx} - \Theta_{xyxy})W_{\text{TT}}^\tau, \quad (3.5)$$

where $W_{\text{TT}} = \frac{1}{2}(\sigma_{\parallel} + \sigma_{\perp})M^2$ and $W_{\text{TT}}^\tau = (\sigma_{\parallel} - \sigma_{\perp})M^2$. We rewrite this expression in terms of the parallel and perpendicular cross sections which leads to

$$\Theta_{\mu_1\mu_2\nu_1\nu_2}W^{\mu_1\mu_2\nu_1\nu_2} = M^2(\Theta_{xxxx}\sigma_{\parallel} + \Theta_{xyxy}\sigma_{\perp}). \quad (3.6)$$

For further calculations it is convenient to express $\Theta_{\mu_1\mu_2\nu_1\nu_2}$ in terms of the transverse momentum tensor T_{ij} defined in eq. (2.15)

$$\Theta_{\mu_1\mu_2\nu_1\nu_2}(\omega_1, \omega_2, \mathbf{b}, \mathbf{k}_{\perp}) = T_{\mu_1\mu_2}(\omega_1, \omega_2, \mathbf{b}, \mathbf{k}_{\perp})T_{\nu_1\nu_2}^*(\omega_1, \omega_2, \mathbf{b}, \mathbf{k}_{\perp}). \quad (3.7)$$

We now treat the important case of central collisions, $\mathbf{b} = 0$, explicitly. In this case the transverse momentum tensor T_{ij} may be written as

$$\begin{aligned} T_{ij}(\omega_1, \omega_2, \mathbf{b} = 0, \mathbf{k}_{\perp}) \\ = \int dq_{1x} dq_{1y} \frac{-q_{1i}q_{1j}}{\left[\left(\frac{\omega_1}{\gamma} \right)^2 + q_{1x}^2 + q_{1y}^2 \right] \left[\left(\frac{\omega_2}{\gamma} \right)^2 + q_{1x}^2 + q_{1y}^2 + k_{\perp}^2 - 2k_{\perp}q_{1x} \right]}, \end{aligned} \quad (3.8)$$

where we suppressed the corresponding form factors for convenience. It follows directly from eq. (3.8) that $T_{xy}(\omega_1, \omega_2, \mathbf{b} = 0, \mathbf{k}_{\perp})$ vanishes identically. Going back to eq. (3.6) we therefore find in the case $\mathbf{b} = 0$:

$$\Theta_{\mu_1\mu_2\nu_1\nu_2}W^{\mu_1\mu_2\nu_1\nu_2} = M^2|T_{xx}|^2\sigma_{\parallel}. \quad (3.9)$$

This result confirms our expectation that only σ_{\parallel} (and not σ_{\perp} or τ_a) enters; this is also in agreement with eq. (2.1), where $\sin \varphi = 0$ for central collisions (see fig. 2).

In the following we explicitly calculate the transverse momentum distribution for the case of $^{208}\text{Pb}-^{208}\text{Pb}$ collisions. To show the basic properties of the transverse momentum distribution we treat the case $\mathbf{b} = 0$ and $Y = 0$. For these conditions the denominator of the transverse momentum tensor eq. (2.15) can be written as (we suppress the index \perp of \mathbf{k}_{\perp} in the following and write $\omega_1 = \omega_2 = \omega$):

$$\left[\left(\frac{\omega}{\gamma} \right)^2 + \left(\frac{1}{2}\mathbf{k} + \mathbf{q} \right)^2 \right] \left[\left(\frac{\omega}{\gamma} \right)^2 + \left(\frac{1}{2}\mathbf{k} - \mathbf{q} \right)^2 \right] = \left[\left(\frac{\omega}{\gamma} \right)^2 + \frac{1}{4}k^2 + q^2 \right]^2 - (\mathbf{k} \cdot \mathbf{q})^2. \quad (3.10)$$

For the form factors entering the transverse momentum tensor we may choose for ^{208}Pb (see ref. [21]):

$$F_{\text{Pb}}^2(Q^2) = \exp\left(-\frac{Q^2}{Q_0^2}\right); \quad Q_0 = 60 \text{ MeV.} \quad (3.11)$$

Introducing polar coordinates, the relevant transverse momentum tensor reads explicitly:

$$\begin{aligned} T_{xx}(\omega, \mathbf{b}=0, k) &= \exp\left[\frac{1}{Q_0^2}\left(\frac{\omega}{\gamma}\right)^2\right] \exp\left[-\frac{k^2}{4Q_0^2}\right] \\ &\times \int_0^\infty q \, dq \exp\left(-\frac{q^2}{Q_0^2}\right) \int_0^{2\pi} d\varphi \frac{\frac{1}{4}k^2 - q^2 \cos^2\varphi}{\left[\left(\frac{\omega}{\gamma}\right)^2 + \frac{1}{4}k^2 + q^2\right]^2 - k^2q^2 \cos^2\varphi} \end{aligned} \quad (3.12)$$

The angular integration in eq. (3.12) can be carried out analytically, leading to two different types of integrals over q :

$$\begin{aligned} T_{xx}(\omega, \mathbf{b}=0, k) &= 2\pi \exp\left[\frac{1}{Q_0^2}\left(\frac{\omega}{\gamma}\right)^2\right] \exp\left(-\frac{k^2}{4Q_0^2}\right) \\ &\times \left(\int_0^\infty \frac{q \exp\left(-\frac{q^2}{Q_0^2}\right) dq}{\left[\left(\frac{\omega}{\gamma}\right)^2 + \frac{1}{4}k^2 + q^2\right] \sqrt{\left[\left(\frac{\omega}{\gamma}\right)^2 + \frac{1}{4}k^2 + q^2\right]^2 - k^2q^2}} \right. \\ &\left. - \int_0^\infty \left[q^3 \exp\left(-\frac{q^2}{Q_0^2}\right) dq \right] / \left\{ \left[\left(\frac{\omega}{\gamma}\right)^2 + \frac{1}{4}k^2 + q^2\right]^2 \right. \right. \\ &\left. \left. - k^2q^2 + \left[\left(\frac{\omega}{\gamma}\right)^2 + \frac{1}{4}k^2 + q^2\right] \sqrt{\left[\left(\frac{\omega}{\gamma}\right)^2 + \frac{1}{4}k^2 + q^2\right]^2 - k^2q^2} \right\} \right). \end{aligned} \quad (3.13)$$

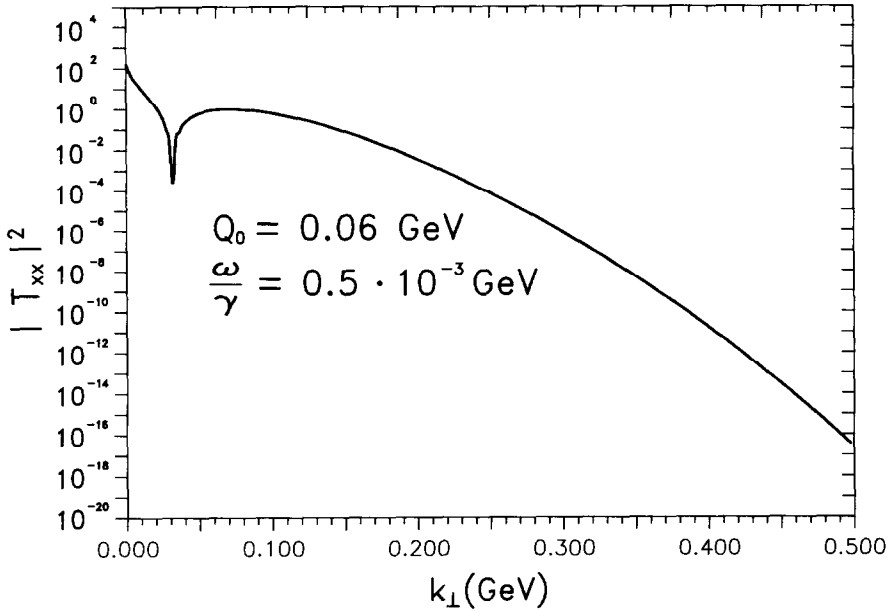


Fig. 3. Dimensionless quantity $|T_{xx}|^2$ [see eq. (3.13)] as a function of the transverse momentum k_{\perp} of the produced system for ^{208}Pb at $b = 0$ and $Y = 0$. The universal ratio ω/γ was set to 0.5×10^{-3} GeV.

In general these integrals can only be solved numerically. For $k = 0$ both integrations can be done completely analytically; the results were used as an additional check on the computer code.

In fig. 3 the dimensionless quantity $|T_{xx}|^2$ is plotted against the transverse momentum of the created system for $\omega/\gamma = 0.5 \times 10^{-3}$ GeV (this corresponds to an invariant mass of about 3.5 GeV at LHC energies and about 0.1 GeV at RHIC energies). From eq. (3.12) it is directly seen that the dependence of the transverse momentum tensor on this universal ratio is very weak for $\frac{1}{2}k \gg \omega/\gamma$. The transverse momentum distribution shows a very strong decrease for increasing transverse momentum. For transverse momenta between 0.1 GeV and 0.5 GeV the transverse momentum distribution decreases about 30 orders of magnitude. The structure for very low values of the transverse momentum is due to a zero of T_{xx} in this region.

In the case of lepton pair production this behaviour makes it possible to distinguish coherent $\gamma\gamma$ -produced pairs from thermal or Drell–Yan pairs. The transverse momentum distributions of these pairs are very broad in a range of 4–5 GeV peaked around zero transverse momentum (see e.g. ref. [2]).

3.2. Coherent $\gamma\gamma$ lepton pair production

The basic relations for the treatment of coherent $\gamma\gamma$ lepton pair production in ultra-relativistic heavy ion collisions are given by eq. (2.1) together with eq. (2.2a,

2.2b). For $\mathbf{b} = 0$, eq. (2.1) can be written in terms of the invariant mass M of the $\gamma\gamma$ system and its rapidity Y as (see ref. [8]):

$$\frac{d^2P(M, Y, b=0)}{dM dY} = \int d^2\boldsymbol{\rho} \frac{2\sigma_{\text{TT}}(M^2)}{M} N(\tfrac{1}{2}M e^Y, \boldsymbol{\rho}) N(\tfrac{1}{2}M e^{-Y}, \boldsymbol{\rho}). \quad (3.14)$$

In principle in the equivalent-photon approximation σ_{TT} is the on-shell photoproduction cross section for transverse photons $\sigma_{\gamma\gamma}$ (Actually, σ_{\parallel} should be used in eq. (3.14) instead of the unpolarized cross section, but in the case of dilepton production this effect is small and can be safely neglected.). For lepton pair production, especially for e^+e^- production, this on-shell approximation is not sufficient (see ref. [9] sect. 6). It is possible to correct $\sigma_{\gamma\gamma}$ due to the off-shell character of the photons via a q^2/M^2 expansion (see ref. [9] eq. (6.25)):

$$\sigma_{\text{TT}}(M^2) = \sigma_{\gamma\gamma}(M^2) \left(1 - \frac{\ln(1+a) + a(1+a)^{-1}}{\ln\left(\frac{M^2}{m_1^2}\right) - 1} \right),$$

$$a = \frac{(m_1^2 - k_1^2)(m_1^2 - k_2^2)}{m_1^2 M^2}. \quad (3.15)$$

The main contribution to the transverse momenta k_1 and k_2 is determined through the size of the colliding nuclei (see sect. 3.1). Therefore it is a good approximation to fix these momenta at

$$k^2 \cong \frac{1}{R^2}, \quad (3.16)$$

where R is the nuclear radius. Fig. 4 shows the off-shell correction function $\sigma_{\text{TT}}/\sigma_{\gamma\gamma}$ for e^+e^- (full line) and for $\mu^+\mu^-$ (dashed line) production as a function of the invariant mass M of the $\gamma\gamma$ system in the case of $^{208}\text{Pb}-^{208}\text{Pb}$ collisions. For invariant masses below 1 GeV, fig. 4 shows the importance of the off-shell correction in the e^+e^- case. In the $\mu^+\mu^-$ case remarkable off-shell effects set in only below 0.5 GeV. This clearly indicates the dependence of the off-shell effects on the ratio M^2/m_1^2 mentioned in ref. [9]. For large invariant masses M the off-shell correction function tends to one.

It is well known [6,11] that there is a very large cross section for the production of e^+e^- -pairs close to the threshold, $M \approx 2m_e \approx 1$ MeV. For every heavy system, this leads to problems with lowest-order perturbation theory [7]. It was shown in ref. [22] (see also ref. [23]) how this problem can be solved by summing a subset of diagrams to infinite order. This problem is not relevant in the present context.

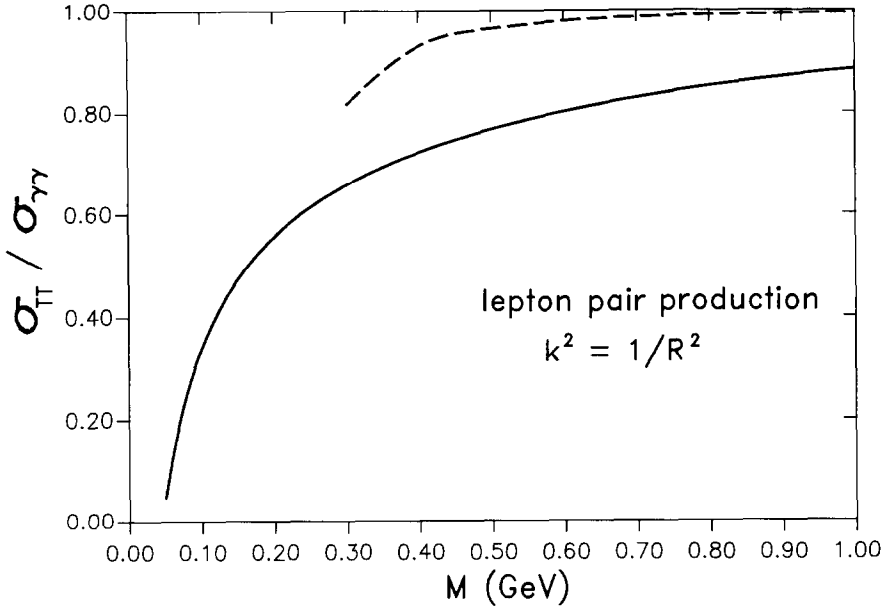


Fig. 4. Off-shell correction function $\sigma_{\text{TT}}/\sigma_{\gamma\gamma}$ for e^+e^- (full line) and $\mu^+\mu^-$ (dashed line) production as a function of the invariant mass M of the $\gamma\gamma$ system for $^{208}\text{Pb}-^{208}\text{Pb}$ collisions.

In fig. 5 and fig. 6 we compare coherent $\gamma\gamma$ lepton pair production probabilities at RHIC and LHC energies in $^{208}\text{Pb}-^{208}\text{Pb}$ central collisions to probabilities of other lepton-pair-production mechanisms, i.e. thermal and Drell–Yan production. The present numerical results can be compared with the calculations of ref. [8], where a low-frequency approximation was made. In the region of applicability of this approximation the agreement between the calculations is good.

In fig. 5 the e^+e^- production probability is plotted as a function of the invariant mass M for RHIC (fig. 5a $\gamma = 100$) and for LHC (fig. 5b $\gamma = 3400$) energies. The full line corresponds to numerical calculations of eq. (3.14) including off-shell corrections via eq. (3.15), while the dashed line shows the thermal production and the dashed-dotted line the Drell–Yan production contribution [2]. Recently, thermal production of low-mass dielectrons in central nucleus–nucleus collisions at LHC energies was also studied in ref. [24]. For RHIC energies (see fig. 5a) the probability distribution for coherent e^+e^- production is well in the range of the other contributions. For energies between 0.5 GeV and 1 GeV the peak structure of the predicted thermal production contribution dominates, while for higher energies this contribution decreases fast. Above 2 GeV the coherent e^+e^- production contribution is larger than the Drell–Yan contribution. Above 4 GeV the coherent e^+e^- production contribution becomes smaller than the Drell–Yan one.

For LHC energies (see fig. 5b) the situation changes only slightly. The region where the thermal contribution decreases below the coherent one is shifted to

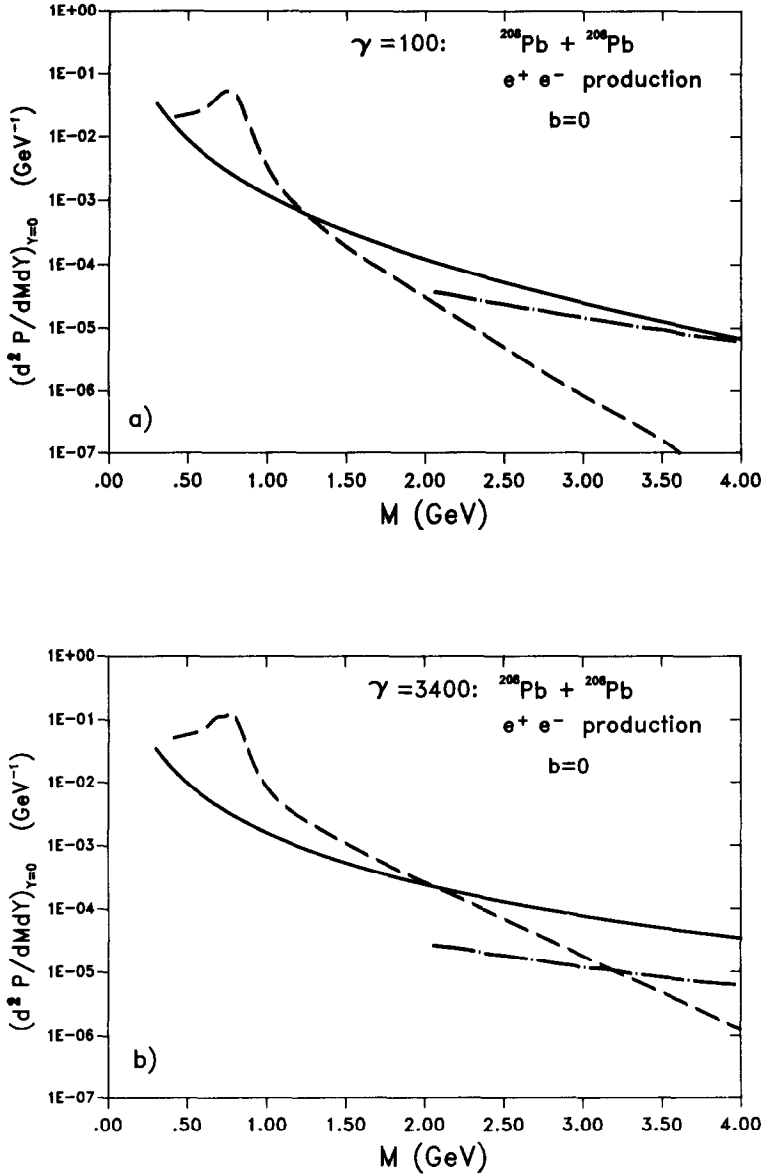


Fig. 5. Differential production probabilities of coherent e^+e^- production (full line) as a function of the invariant mass M in central ($b=0$) $^{208}\text{Pb}-^{208}\text{Pb}$ collisions in comparison to thermal (dashed line) and Drell-Yan (dashed dotted line) production. (a) Double differential production probabilities for RHIC energies. (b) Double differential production probabilities for LHC energies.

higher invariant masses of about 2 GeV . While the Drell-Yan production contribution seems not to be very much affected by the increase of the Lorentz factor γ , the thermal and the coherent e^+e^- production contributions are enhanced. This

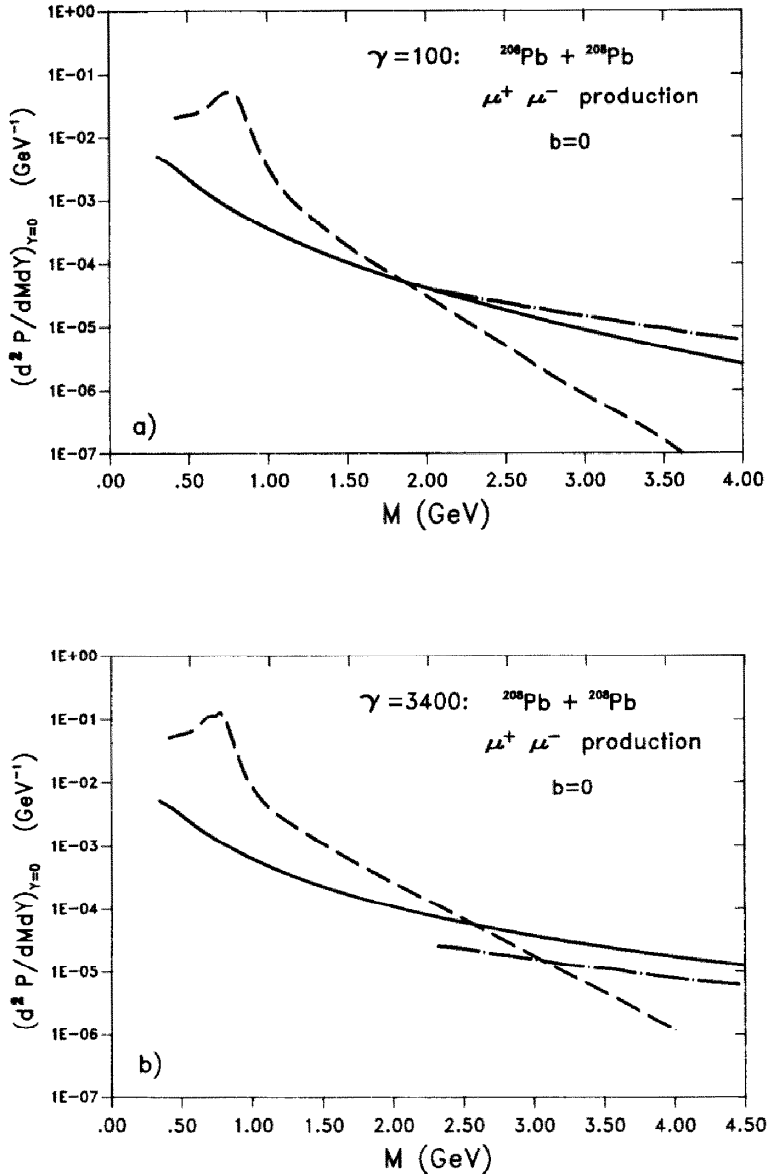


Fig. 6. Differential production probabilities of coherent $\mu^+ \mu^-$ production (full line) as a function of the invariant mass M in central ($b = 0$) $^{208}\text{Pb}-^{208}\text{Pb}$ collisions in comparison to thermal (dashed line) and Drell-Yan (dashed dotted line) production. (a) Double differential production probabilities for RHIC energies. (b) Double differential production probabilities for LHC energies.

results in a clear dominance of these contributions below 3 GeV. Even above 3 GeV the decrease of the coherent e^+e^- production contribution is very slow, shifting a possible Drell-Yan dominance to very high invariant masses.

For the coherent $\mu^+\mu^-$ production probability (fig. 6) we find qualitatively the same situation as for the e^+e^- production. For RHIC energies (see fig. 6a), because of the higher mass of the muon, the decrease of the thermal production contribution below the coherent production contribution does not set in until an invariant mass of 2 GeV. In contrast to the e^+e^- case, for coherent $\mu^+\mu^-$ production the Drell–Yan production dominates above 2.5 GeV.

For LHC energies (see fig. 6b) the thermal and the coherent production contributions are enhanced in such a way that below 2.5 GeV the thermal contribution dominates but above 2 GeV the coherent one dominates. As a result of this enhancement the Drell–Yan production contribution is smaller than the coherent one even at higher invariant masses.

We now turn to the calculation of differential cross sections from eq. (3.14). For such calculations eq. (3.14) has to be generalized and integrated over impact parameters resulting in:

$$\begin{aligned} \frac{d^2\sigma}{dM dY} &= 2\pi \int_0^\infty b_1 db_1 \int_0^\infty b_2 db_2 \int_0^{2\pi} d\varphi \frac{2\sigma_{\text{TT}}(M^2)}{M} \\ &\times T_i(b) N(\tfrac{1}{2}M e^Y, b_1) N(\tfrac{1}{2}M e^{-Y}, b_2). \end{aligned} \quad (3.17)$$

Because of the explicit treatment of the impact-parameter dependence of the photon spectra the function T_i can characterize the type of collision: For $T_<(b) = \Theta(2R - b)$ the two colliding nuclei overlap and strong interactions take place in addition to the electromagnetic ones; we call these types of collisions disruptive collisions. The pure electromagnetic processes can be studied in non-disruptive collisions characterized by $T_>(b) = \Theta(b - 2R)$. The total production cross section is given by $T_i(b) \equiv 1$. The authors of ref. [12] used $T_<$ and T_i as a convenient way to calculate non-disruptive cross sections. In our framework with extended charge distributions [see eq. (2.2a,b)] this is not applicable; therefore we explicitly calculate the different parts.

The explicit structure of the photon spectra enables us to calculate a differential probability distribution as a function of the impact parameter b of the colliding nuclei (see fig. 1). Rewriting eq. (3.17),

$$\frac{d^2\sigma}{dM dY} = 2\pi \int_0^\infty b db T_i(b) \frac{d^2P(b)}{dM dY}, \quad (3.18)$$

we obtain after changing integration variables

$$\begin{aligned} \frac{d^2P(b)}{dM dY} &= \frac{2\sigma_{\text{TT}}(M^2)}{M} \int_0^\infty b_1 db_1 N(\tfrac{1}{2}M e^Y, b_1) \\ &\times \int_0^{2\pi} d\psi N[\tfrac{1}{2}M e^{-Y}, b_2(b_1, \psi)] \end{aligned} \quad (3.19)$$

From eq. (3.18) the development of the coherent lepton pair production probability from disruptive to non-disruptive collisions can be studied explicitly.

In fig. 7 the coherent e^+e^- production probability is plotted as a function of the impact parameters b of the colliding nuclei for $^{208}\text{Pb}-^{208}\text{Pb}$ collisions at SPS and

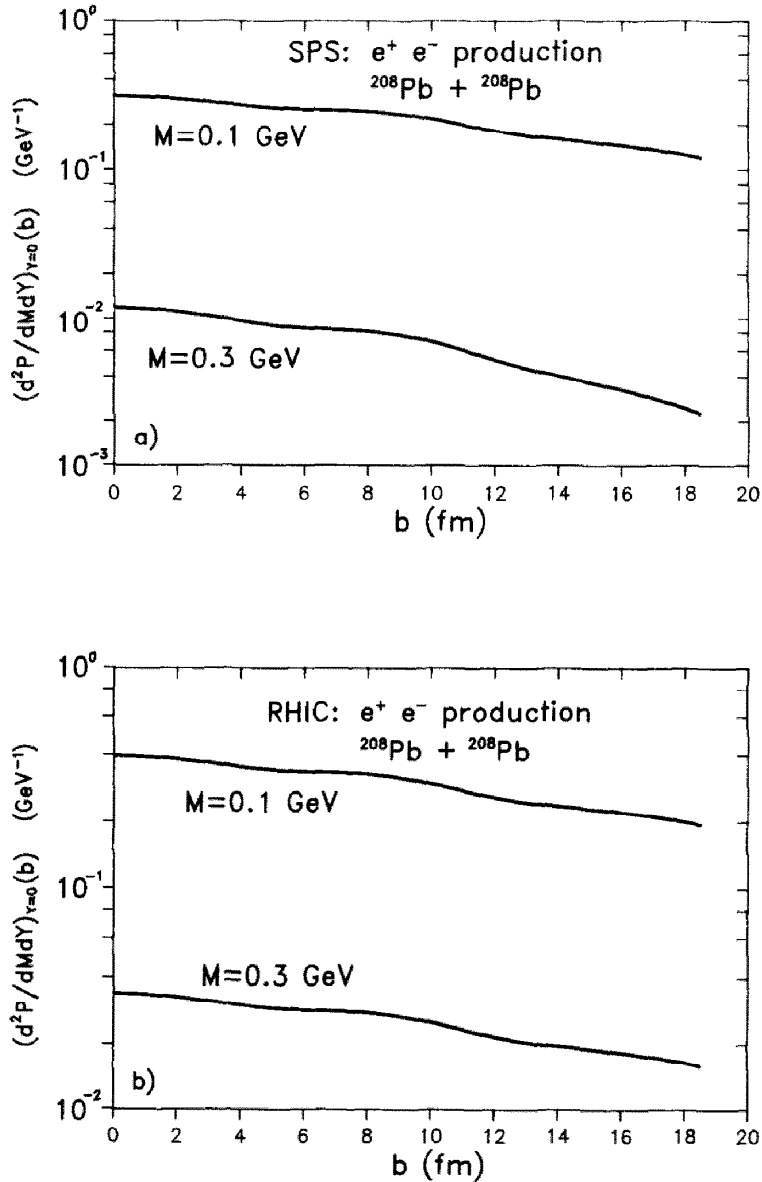


Fig. 7. Differential production probabilities of coherent e^+e^- production as a function of the impact parameter b in $^{208}\text{Pb}-^{208}\text{Pb}$ collisions. For $Y=0$ the probability distributions are plotted for two characteristic values of the invariant mass M . (a) Double differential production probability for SPS energies. (b) Double differential production probability for RHIC energies.

RHIC energies. For $Y = 0$ we plotted the distributions for the two characteristic values of the invariant mass M .

For SPS (see fig. 7a) as well as for RHIC energies (see fig. 7b) the probability distributions smoothly decrease from a maximum value at $b = 0$. The distributions vary slowly and there are no significant characteristics at $b = 2R$. The absolute values of the probability distribution for RHIC energies are enhanced and the decrease for large b is not as strong as compared to SPS.

To calculate differential cross sections one can evaluate either eq. (3.17) or eq. (3.18). A comparison between the results of both equations was used as a check for the computer codes. Under purely numerical aspects it is advantageous to use eq. (3.17) for the several differential cross sections.

Fig. 8 shows the results for the differential cross sections for coherent e^+e^- production at $Y = 0$ as a function of the invariant mass M at SPS, RHIC and LHC energies. Below 0.5 GeV all differential cross sections are of the order of b/GeV to mb/GeV . Above 1 GeV the cross section for SPS energies decreases very fast while the others still contribute. This is a result of the general fact that for increasing Lorentz factor the available invariant mass regions also increase.

In fig. 8a the differential cross section for disruptive collisions at SPS, RHIC and LHC energies is shown. For low invariant masses all cross sections tend to the same values. The cross sections for LHC and RHIC do not differ significantly below 1 GeV. This is a result of the saturation property for disruptive collisions for increasing Lorentz factors mentioned in ref. [8]. The difference to the SPS cross section increases to several orders of magnitude for higher invariant masses.

Fig. 8b shows the differential cross sections for non-disruptive collisions. All cross sections are enhanced nearly one order of magnitude in comparison to the disruptive ones. This is a result of the unrestricted impact-parameter range for those collisions. For the same reason the saturation property for disruptive collisions is not observed for non-disruptive ones: For very low values of the invariant mass, the cross sections for RHIC and LHC energies do tend to the same value, but for invariant masses above 0.3 GeV they are well separated. For invariant masses above 1 GeV the LHC cross section is more than one order of magnitude bigger than the RHIC cross section which itself is several orders of magnitude bigger than the SPS one.

So far in the calculations of disruptive and non-disruptive collisions we chose a simple sharp cut-off $T_<$ and $T_>$ in eq. (3.17) to describe the set in of the strong absorption effect. It seems to be more realistic to assume a smooth function T_s which describes the gradual set-in of strong absorption as proposed in ref. [11]. For first calculations it is sufficient to take a well-known Fermi function

$$T_s(b) = \left[1 + \exp\left(\frac{b - 2R}{z}\right) \right]^{-1}, \quad (3.20)$$

where z is the thickness parameter.

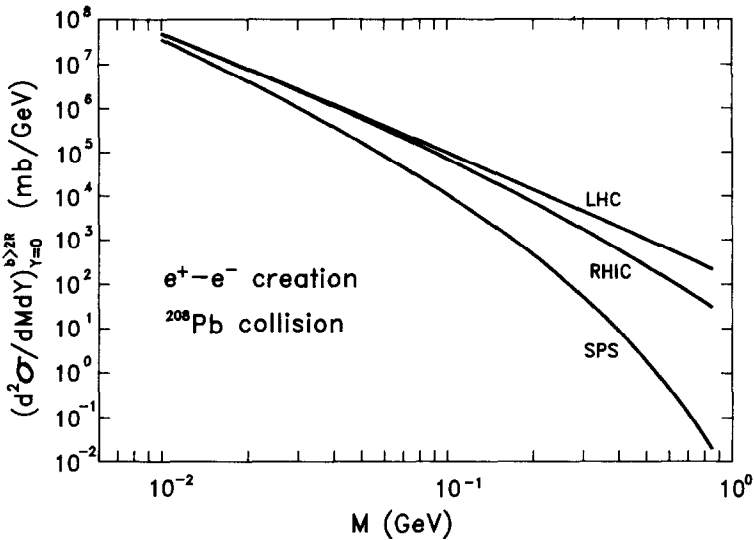
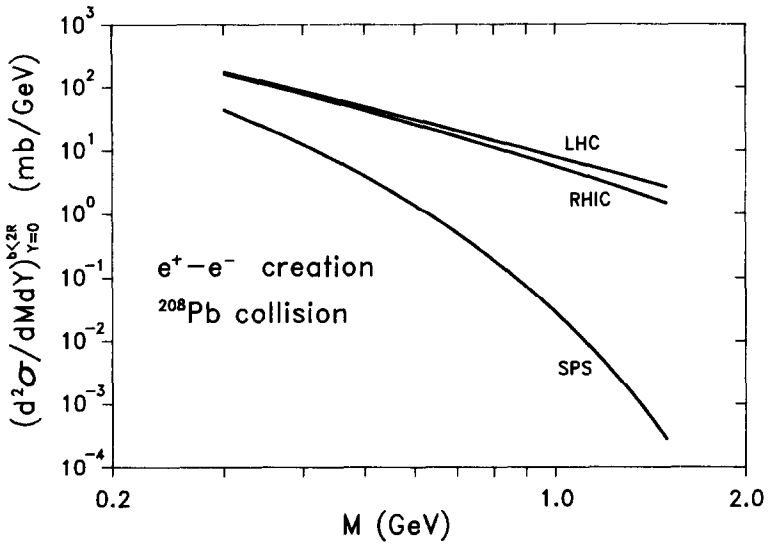


Fig. 8. Differential cross sections of coherent e^+e^- production as a function of the invariant mass M for $Y=0$ in ^{208}Pb - ^{208}Pb collisions. Collisions at SPS, RHIC and LHC are mentioned. (a) Double differential cross sections for disruptive collisions at SPS, RHIC and LHC energies. (b) Double differential cross sections for non-disruptive collisions at SPS, RHIC and LHC energies.

In fig. 9 we plotted the differential e^+e^- production cross section at $Y=0$ for disruptive ^{208}Pb - ^{208}Pb collisions at RHIC energies as a function of the invariant mass M . The full line corresponds to a calculation in the sharp cut-off model using

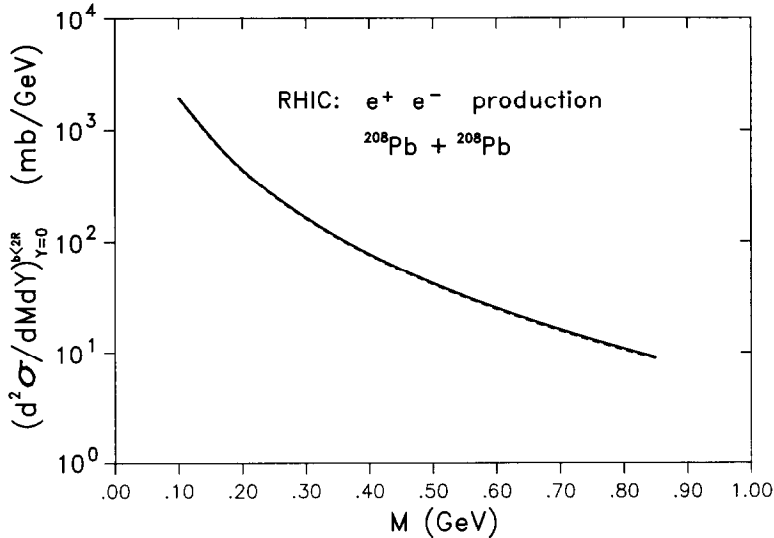


Fig. 9. Differential cross section of coherent e^+e^- production as a function of the invariant mass M for $Y=0$ in $^{208}\text{Pb}-^{208}\text{Pb}$ collisions. The full line corresponds to a sharp cut-off model using $T_<$, while the dashed line corresponds to a smooth cut-off model using T_s for the set in of strong absorption effects.

$T_<$, while the dashed line corresponds to the smooth set-in of strong absorption using T_s with $z = 2$ fm. The comparison between the two calculations shows that the introduction of a smooth set-in of strong absorption effects does not affect the differential cross section significantly; a very small shift to lower values is obtained. This is in accordance with fig. 7a, b: The very smooth and slow decrease of the impact-parameter-dependent probability distribution makes eq. (3.18) very insensitive to small changes in the integration. Because of the monotony of the probability distributions the smooth cut-off gives somewhat smaller results.

4. Conclusions

Coherent $\gamma\gamma$ lepton pair production in ultra-relativistic heavy-ion collisions was studied theoretically in the framework of the equivalent-photon method. The basic relation between the production probability and the impact-parameter-dependent equivalent-photon spectra was derived from first principles within the semiclassical method. In our calculation we did not specify the internal process $\gamma\gamma \rightarrow f(k)$ but introduced general amplitudes applicable to every internal process. This is a generalization of the method used e.g. in refs. [25,26], where especially the $\gamma\gamma$ production of 0^+ and 0^- states was considered.

From our derivation we obtained a transverse momentum distribution tensor of the produced system in a straightforward way. We have seen that the k_{\perp} -distributions are sharply peaked around zero with a width of the order of $Q_0 \cong 1/R$ for central collisions. For distant collisions this width will be even smaller, of the order of $1/b$. The transverse momentum distribution for the coherent pairs is very sharply peaked around zero which leads to the possibility to distinguish them from lepton pairs produced in other mechanisms, like thermal or Drell–Yan production.

We gave numerical results for the coherent $\gamma\gamma$ lepton pair production at SPS, RHIC and LHC energies. We compared differential probabilities for coherent e^+e^- and $\mu^+\mu^-$ production to the ones from thermal and Drell–Yan production over a wide range of invariant masses. The probability distributions are of comparable order of magnitude.

Purely impact-parameter-dependent differential probability distributions were calculated. The consistent treatment of the equivalent-photon spectra leads to a smooth, decreasing distribution over a wide range of impact parameter values. This explicit treatment of the impact parameter dependence of the photon spectra enables us to distinguish between disruptive (with strong interactions) and non-disruptive (pure electromagnetic interactions) collisions. Calculations of differential cross sections for both cases were carried out. Resulting cross sections are very large; main contributions originate from the non-disruptive collisions. With increasing Lorentz factor the cross sections of the non-disruptive collisions are more and more enhanced, while for disruptive collisions a saturation effect sets in. We introduced, besides the sharp cut-off model for the strong absorption effects, a smooth cut-off model. Numerical calculations indicate an insensitivity of the differential cross sections for such model variations.

Several types of differential cross sections which are of interest are left for numerical calculations of coherent lepton pair production in the future. The general formulation of the equivalent-photon method leads to the possibility to calculate differential probability distributions and cross sections for the coherent production of other systems, like the Higgs boson. Effects of stopping from strong interactions in disruptive collisions are not treated so far. These stopping effects (expected to be more important at SPS than at RHIC or LHC energies) will modify the equivalent photon spectra in a characteristic way. In turn, this will be reflected in the dilepton distribution. Therefore $\gamma\gamma$ dileptons could develop into a tool to investigate the time development of the colliding nuclear charge distributions.

In our work we obtained a reliable guide to the characteristics of coherent γ lepton pair production and their impact-parameter dependence in relativistic heavy-ion collisions.

One of the authors (N.B.) would like to thank the Studienstiftung des deutschen Volkes for the support of his studies.

References

- [1] E.V. Shuryak, The QCD vacuum, hadrons and the superdense Matter, Lecture Notes in Physics, Vol. 8 (World Scientific, Singapore, 1988)
- [2] P.V. Ruuskaanen, Proc. Large hadron collider workshop, Aachen, Oct. 4–9, 1990, vol. II, p. 1164, eds. G. Jarlskog and D. Rein, CERN 90-10
- [3] L.D. Landau and E.M. Lifshitz, Phys. Sz. Sowjet 6 (1934) 244
- [4] G. Soff in Proc. 18th winter school eds. A. Balanda and Z. Stachura, (Bielsko-Biala, Poland, 1980) p. 201
- [5] U. Becker, N. Grün and W. Scheid, J. Phys. B19 (1986) 1347
- [6] G. Alexander, E. Gotsman and U. Maor, Z. Phys. C34 (1987) 329
- [7] C.A. Bertulani and G. Baur, Phys. Reports 163 (1988) 299
- [8] G. Baur, Z. Phys. C, Z. Phys. C54 (1992) 419
- [9] V.M. Budnev et al., Phys. Reports 15 (1974) 182
- [10] G. Baur, Strong electromagnetic fields in relativistic heavy ion collisions, invited talk, CBPF International Workshop on relativistic aspects of nuclear physics (Rio de Janeiro, Brazil, Aug. 1989) ed. T. Kodama et al. (World Scientific, Singapore, 1990) p. 127; invited talk, 6th nordic Meeting on nuclear physics (Haugesund, Norway, August 1989) Phys. Scr. T32 (1990) 76
- [11] G. Baur and L.G. Ferreira Filho, Nucl. Phys. A518 (1990) 786
- [12] N. Cahn and J.D. Jackson, Phys. Rev. D42 (1990) 3690
- [13] J. Norbury, Phys. Rev. D42 (1990) 3696
- [14] E. Papageorgui, Phys. Lett. B250 (1990) 155
- [15] B. Müller and A.J. Schramm, Phys. Rev. D42 (1990) 3699
- [16] C. Bottcher and M.R. Strayer, Nucl. Phys. A544 (1992) 255c
- [17] G. Baur and L.G. Ferreira Filho, Phys. Lett. B254 (1991) 30
- [18] A.I. Akhiezer and V.B. Berestetskii, Quantum electrodynamics (Interscience, and New York, 1965)
- [19] G. Bonneau, M. Gourdin and F. Martin, Nucl. Phys. B54 (1973) 573
- [20] N. Baron and G. Baur, contribution to EPS 9, Trends in physics, Firenze, Italy
- [21] M. Drees, J. Ellis and D. Zeppenfeld, Phys. Lett. B223 (1989) 454
- [22] G. Baur, Phys. Rev. A42 (1990) 5736
- [23] M.J. Rhoades-Brown and J. Weneser, Phys. Rev. A44 (1991) 330
- [24] J. Cleymans, K. Redlich and H. Satz, Z. Phys. C52 (1991) 517
- [25] G. Soff, W. Michelbach, M. Greiner, M. Vidovic, Ch. Best, S. Schneider, D. Hilberg and Ch. Hoffmann, Proc. 7th adriatic Int. Conf. on nuclear physics, 1991, Islands of Brioni, Croatia, May 27–June 1, ed. R. Caplar and W. Greiner (1991) p. 353
- [26] M. Vidovic, GSI-91-32, September 1991